Malaysian Journal of Mathematical Sciences 20(3): 955–972 (2026)
https://doi.org/10.47836/mjms.20.3.05

Malaysian Journal of Mathematical Sciences

Journal homepage: https://mjms.upm.edu.my

Peristaltic Transport of a Rabinowitsch Fluid with Suction and Injection Through a Permeable Wall Under Slip Conditions: Applications in Biomedical and Industrial Systems

Sivaranjani, S.[1] and Kavitha, A.[1*]

[1]*Department of Mathematics, School of Advanced Sciences, Vellore Institute of Technology, Vellore, 632014, India.*

E-mail: kavitha@vit.ac.in
[*]Corresponding author

Received: 1 July 2025
Accepted: 12 December 2025

Abstract

Efficient peristaltic transport of non-Newtonian fluids plays a vital role in biomedical, industrial, and microfluidic applications such as drug delivery, dialysis, polymer processing, and filtration. This study investigates the peristaltic motion of a Rabinowitsch fluid through a permeable channel, focusing on the combined effects of suction/injection, wall slip, and permeability on pressure rise, velocity distribution, and frictional forces. Analytical solutions are derived using lubrication theory under the assumptions of long wavelength and low Reynolds number, while MATLAB simulations are employed to examine the influence of key parameters. The results show that suction/injection enhances pressure rise, slip parameters (β_1, β_2) distinctly regulate flow resistance and velocity distribution, and higher wall permeability induces nonlinear velocity growth. These findings offer valuable insights for optimizing fluid transport and improving energy efficiency in biomedical and industrial systems.

Keywords: Rabinowitsch fluid, peristaltic transport, suction and injection, slip condition, permeable wall.

1 Symbols and Abbreviations

Symbol/Abbreviations	Description
b	Amplitude of the wave
ϕ	Amplitude ratio
Q	Average non-dimensional flow rate
g	Gravitational acceleration vector
a	Half-width of the channel
P	Pressure
v	Kinematic viscosity
Re	Reynolds number
β_1, β_2	Slip parameters
k	Suction/Injection parameter
t	Time
v_0	Velocity
(U, V)	Velocity components in lab frame
(u, v)	Velocity components in wave frame
μ	Dynamic viscosity
δ	Wave number parameter
c	Wave speed
τ_{xx}	Normal stress in x-direction
τ_{yy}	Normal stress in y-direction
τ_{xy}	Shear stress on plane normal to x acting in y-direction
τ_{yx}	Shear stress on plane normal to y acting in x-direction

2 Introduction

Peristaltic transport is a fundamental mechanism in physiological and engineering systems, enabling the movement of fluids through periodic contractions of flexible walls. In biological contexts, it governs vital processes such as blood circulation, digestion, and urine transport. Since blood and other biological fluids exhibit non-Newtonian characteristics, classical Newtonian models are inadequate for describing their dynamics. The Rabinowitsch fluid model, in particular, captures both shear-thinning and shear-thickening behaviors, making it a more accurate representation of complex fluids like blood. Peristaltic processes in the human circulatory system ensure unidirectional blood flow, enabling effective nutrient and oxygen transport. Disturbances in these processes can cause cardiovascular problems. Studying peristaltic transport with wall suction/injection, and slip is essential for improving diagnostic and therapeutic techniques.

Abbas et al. [1] studied peristaltic motion of Jeffrey fluid in a permeable channel under Lorentz force and chemical reactions. Magnetic fields and chemical reactions significantly influence mass transfer and velocity profiles. Abd-Alla et al. [2] investigated the magnetohydrodynamic peristaltic transport of Jeffrey fluid in an asymmetric porous channel with heat transfer effects. Their results highlight how magnetic field, porosity, and thermal conditions influence velocity and temperature distributions. Akbar et al. [3] investigated heat transfer in Rabinowitsch fluid flow driven by metachronal ciliary waves. Analytical solutions for temperature and Nusselt number showed that increasing wave amplitude enhances heat transfer; effects vary with fluid rheology.

Akram et al. [4] investigated peristaltic transport of Maxwell fluid in a porous asymmetric channel. Solutions for velocity and pressure gradient show the effects of porosity, asymmetry, and fluid relaxation time on flow behavior. Aly and Ebaid [5] presented an exact solution for the peristaltic transport of nanofluids in an asymmetric channel under the influence of a second-order velocity slip condition. Their study demonstrates how slip effects significantly alter the flow and heat transfer characteristics. Chakradhar et al. [6] explored MHD peristaltic motion of Williamson fluid in a porous channel with suction and injection. Permeability, suction/injection, and magnetic field strongly affect flow, relevant for industrial and biomedical devices.

Chamkha et al. [7] studied unstable heat and mass transfer from a stretched surface in a porous medium with chemical reactions and suction/injection. Showed how these factors affect temperature and concentration profiles for industrial applications. Channakote and Kalse [8] investigated heat transfer in peristaltic flow of Rabinowitsch fluid through a conduit with porous walls. Fluid properties and wall permeability significantly influence temperature distribution and heat transfer. El Shehawey and Husseny [9] analyzed peristaltic flow through a porous medium considering the effects of porous boundaries. Their study showed that wall permeability significantly influences the velocity and pressure distribution within the channel. Elmhedy et al. [10] investigated the effects of heat transfer and an inclined magnetic field on peristaltic flow of an incompressible Rabinowitsch fluid in an inclined channel using lubrication approximation. Results show heat transfer and magnetic field influence velocity and particle motion, relevant for modelling gastric flow in endoscopic procedures.

Goud et al. [11] investigated peristaltic transport of a pseudoplastic fluid in a tube with permeable walls under suction and injection. Increasing the suction/injection parameter reduces the pressure rise required for pumping, useful for controlling flow in biomedical and industrial applications. Hayat et al. [12] analyzed the simultaneous effects of slip and heat transfer on peristaltic flow, demonstrating the role of slip conditions in modifying velocity and thermal distributions.

Ismail et al. [13] performed a stability analysis of stagnation-point flow with heat transfer over an exponentially shrinking sheet, demonstrating how heat generation influences flow stability and thermal behavior, which supports the importance of stability considerations in mathematical modeling of transport phenomena. Kamisli [14] studied laminar flow of non-Newtonian fluid in channels with wall suction/injection. Analytical solutions for velocity and pressure illustrate how wall suction/injection impacts flow stability and transition, relevant for membrane and filtration systems. Kumar et al. [15] investigated the influence of slip effects on the peristaltic transport of a Rabinowitsch fluid in a non-uniform tube, showing how slip parameters significantly alter the velocity and pressure characteristics of the flow. Lin et al. [16] analyzed Rabinowitsch fluid in power-law film slider bearings. Developed a non-Newtonian Reynolds equation and showed that flow behavior index and layer thickness ratio significantly influence load-carrying capacity and frictional force.

Maiti et al. [17] studied peristaltic blood flow in micro-vessels using a Herschel-Bulkley model. Found that amplitude ratio, fluid index, and vessel shape strongly affect velocity, wall shear stress, flow reversal, and peristaltic pumping efficiency. Misra et al. [18] studied the peristaltic transport of a physiological fluid in an asymmetric porous channel under an applied magnetic field. They examined how the magnetic field and porosity affect the velocity and pressure distribution. Their findings provide insights into magnetohydrodynamic effects on biofluid flow in physiological channels. Misra et al. [19] explored peristaltic transport of a non-Newtonian fluid with a peripheral layer. Using long wavelength and low Reynolds assumptions, higher outer layer viscosity was found to increase pressure and frictional forces, depending on fluid rheology. Rafiq and Abbas [20] examined heat radiation and viscous dissipation effects on Rabinowitsch fluid flow in a non-uniform inclined tube with convective slip. Analytical results show strong influence of thermal radiation and viscous dissipation on temperature and flow behavior. Rajashekhar et al.

[21] explored unstable peristaltic transport of Rabinowitsch fluid in a non-uniform channel with temperature-dependent fluid properties. Temperature variation significantly affects pressure distribution and velocity profiles.

Ramamoorthy and Pallavarapu [22] investigated the second-order slip effects on the flow of a conducting Jeffrey nanofluid in an inclined asymmetric porous channel. Sadaf and Nadeem [23] explored peristaltic transport of Rabinowitsch fluid in a non-uniform tube with convective boundary conditions and viscous dissipation. Found that velocity increases with stiffness, rigidity, and viscous damping for shear-thinning fluids, while Brinkman number enhances temperature. Saravana et al. [24] studied peristaltic pumping in an inclined channel with compliant walls, considering heat transfer. Derived expressions for velocity, temperature, and heat transfer coefficient; fluid index and wall compliance impact flow and trapping. Satwai et al. [25] studied blood flow with nanoparticles through a porous inclined overlapping stenosed artery under an external magnetic field and demonstrated how porosity, magnetic field strength, and nanoparticle effects significantly influence velocity distribution and wall shear stress, providing a mathematical basis for incorporating porous media and non-Newtonian effects in physiological flow models. Shapiro et al. [26] examined peristaltic pumping using lubrication approximation. Demonstrated that wave-induced motion can drive flow without external pressure, providing foundational understanding for flow in flexible biological conduits.

Singh et al. [27] conducted a theoretical study on heat transfer in peristaltic transport of a Rabinowitsch fluid, analyzing the influence of non-Newtonian behavior and peristaltic motion on velocity and temperature distributions in a channel. Sivaranjani and Kavitha [28] analyzed the peristaltic transport of a pseudoplastic fluid under MHD effects with first-order slip conditions at permeable walls. Their results provide insights for designing efficient peristaltic pumping systems in non-Newtonian fluid applications. Srinivas et al. [29] examined the effects of slip conditions, wall properties, and heat transfer on MHD peristaltic transport, highlighting how these factors significantly influence flow behavior and thermal characteristics. Tripathi [30] studied peristaltic transport of a viscoelastic fluid using the fractional Maxwell model. Analytical expressions for velocity, pressure, and shear force showed that increasing fractional parameter and relaxation time decreases pressure difference, aiding analysis of viscoelastic flows. Vaidya et al. [31] investigated peristaltic flow in an inclined porous channel with convective boundary conditions. Rheology of shear-thinning and shear-thickening fluids is strongly affected by fluid properties; porosity reduces trapping for Newtonian and dilatant fluids but increases it for pseudoplastic fluids. Yu-Ming et al. [32] investigated entropy generation in Rabinowitsch fluid flow through an inclined wavy channel with constant and variable fluid properties. Examined factors affecting thermodynamic efficiency, entropy creation, and heat transfer.

Most studies consider suction/injection or wall slip separately, often focusing on Newtonian or simple power-law fluids. The combined effect of suction/injection, and slip parameters on Rabinowitsch fluid peristaltic transport remains less explored. This study extends the analysis by incorporating both slip and suction/injection parameters to better model physiological applications, including drug transport, cardiovascular diagnostics, and biomedical device design.

Motivated by these considerations, the present study investigates the peristaltic transport of a Rabinowitsch fluid through a permeable wall under the influence of suction/injection and slip conditions. By employing the long wavelength and low Reynolds number approximations, analytical solutions are derived for the velocity distribution, pressure gradient, and frictional force. The influence of key governing parameters including slip, suction/injection parameter, and fluid index is systematically analyzed. The findings provide new insights into flow regulation mechanisms, with potential applications in biomedical engineering, microfluidic devices, and industrial fluid transport systems.

3 Mathematical Formulation

In this study, the peristaltic flow of a Rabinowitsch fluid is considered in a channel of total width $2a$ with permeable walls on both sides. As illustrated in Figure 1, the fluid enters the d omain through the lower wall with a uniform injection velocity v_0 and is removed through the upper boundary at the same rate. The analysis is made simpler by focussing just on the channel's semi-width.

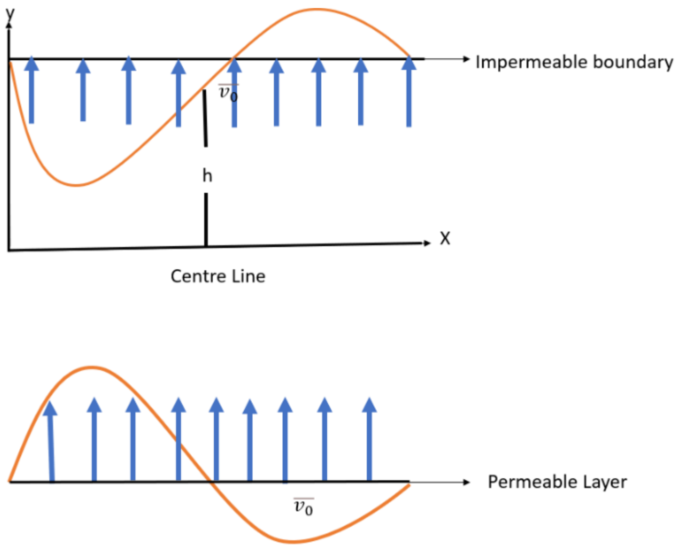

Figure 1: Physical Model

The wall deformation is characterized as.

$$Y = H(X,t) = a + bcos\frac{2\Pi}{\lambda}(X - ct'). \tag{1}$$

where a is half channel width, b is the amplitude of the wave, t' is time, λ is the wavelength.

4 Governing Equations and Boundary Conditions

A well-recognized method to examine the non-Newtonian behavior of a fluid is provided by the Rabinowitsch fluid model, which relates shear stress to shear rate as follows.

$$\tau_{YY} + \alpha\,\tau_{yx}^{3} = \mu\frac{\partial u}{\partial Y}. \tag{2}$$

The continuity and momentum equations for incompressible Rabinowitsch fluid flow in a fixed frame are given by

$$\frac{\partial U}{\partial X}+\frac{\partial V}{\partial Y}=0, \tag{3}$$

$$\rho\left(\frac{\partial U}{\partial t'}+U\frac{\partial U}{\partial X}+V\frac{\partial U}{\partial Y}\right)=-\frac{\partial p}{\partial X}+\frac{\partial \tau_{XX}}{\partial X}+\frac{\partial \tau_{YX}}{\partial Y}, \tag{4}$$

$$\rho\left(\frac{\partial V}{\partial t'}+U\frac{\partial V}{\partial X}+V\frac{\partial V}{\partial Y}\right)=-\frac{\partial p}{\partial Y}+\frac{\partial \tau_{XY}}{\partial X}+\frac{\partial \tau_{YY}}{\partial Y}. \tag{5}$$

Transformation to the wave frame: To simplify the analysis for peristaltic motion, we move to a frame traveling with speed c:

$$\begin{aligned} u' &= U-c,\\ y' &= Y,\\ x' &= X-ct',\\ v' &= V. \end{aligned} \tag{6}$$

Here, u', x', v', and y' represent the axial velocity, axial position, transverse velocity, and transverse position, respectively measured in the wave frame.
Dimensionless variables: The following non-dimensional variables are introduced:

$$\begin{aligned} &u=\frac{u'}{c},\quad v=\frac{v'}{c\delta},\quad x=\frac{x'}{\lambda},\quad y=\frac{y'}{a},\quad h=\frac{H}{a},\quad \delta=\frac{a}{\lambda}, p=\frac{p'a^2}{\mu c\lambda},\quad Re=\frac{\rho ac}{\mu},\\ &t=\frac{ct'}{\lambda},\quad \phi=\frac{b}{a},\quad \tau_{xy}=\frac{a\tau'_{xy}}{c\mu},\quad \tau_{xx}=\frac{a\tau'_{xx}}{c\mu},\quad \tau_{yy}=\frac{a\tau'_{yy}}{c\mu},\quad \alpha=\frac{c^2\mu^2}{a}\gamma. \end{aligned} \tag{7}$$

Assumptions and simplifications: Under the assumptions of long wavelength ($\delta \ll 1$) and low Reynolds number ($Re \ll 1$) [26], the inertia terms are negligible.
Then the governing equations reduce to:

$$\tau_{yx}+\alpha\tau_{yx}^3=\frac{\partial u}{\partial y}, \tag{8}$$

$$\frac{\partial \tau_{yx}}{\partial y}-k\frac{\partial u}{\partial y}=\frac{\partial p}{\partial x}, \tag{9}$$

$$\frac{\partial p}{\partial y}=0. \tag{10}$$

Wave-frame boundary conditions: The equivalent dimensionless boundary conditions in the wave frame are [26]:

$$\frac{\partial u}{\partial y}=0,\quad \frac{\partial^2 u}{\partial y^2}=0 \quad \text{at} y=0, \tag{11}$$

$$u=-1-\beta_1\frac{\partial u}{\partial y}-\beta_2\frac{\partial^2 u}{\partial y^2} \quad \text{at } y=h=1+\phi\cos 2\pi x. \tag{12}$$

Volume flow rate: The volume flow rate in the fixed (Q') and wave (q') frames are defined as:

$$Q'=\int_0^H U\,dy,\quad q'=\int_0^H U\,dy. \tag{13}$$

Using the transformation from fixed to wave frame (Eq. 6), we have

$$Q' = q' + cH. \tag{14}$$

Time-averaged flow: The mean flow over a wave period $T = \lambda/c$ is

$$\hat{Q} = \frac{1}{T}\int_0^T \bar{Q}\,dt = g' + ca. \tag{15}$$

In dimensionless form, this becomes

$$Q = q + 1, \tag{16}$$

where

$$q = \frac{q'}{ac} = \int_0^h u\,dy, \quad Q = \frac{\hat{Q}}{ac}. \tag{17}$$

5 Solution of The Problem

Using the boundary conditions (11) and (12) to solve Eqn (9), we obtain

$$\begin{aligned} u = -1 + \Big(\frac{dp}{dx}\Big)\Big(\frac{y^2-h^2}{2}\Big) - k\Big(\frac{y^3-h^3}{6}\Big) + 3\alpha\Big[\Big(\frac{dp}{dx}\Big)^3\Big(\frac{y^4-h^4}{4}\Big) - 3\Big(\frac{dp}{dx}\Big)^2 k\Big(\frac{y^5-h^5}{10}\Big) + \\ \Big(\frac{dp}{dx}\Big)k^2\Big(\frac{y^7-h^7}{28}\Big) - \beta_1\Big[\Big(\frac{dp}{dx}\Big)h - \frac{k}{2}h^2 + 3\alpha\Big(\Big(\frac{dp}{dx}\Big)^3 h^3 - 3\Big(\frac{dp}{dx}\Big)^2 k\frac{h^4}{2} + 3\Big(\frac{dp}{dx}\Big)k^2\frac{h^6}{4}\Big)\Big] \\ - \beta_2\Bigg[\Big(\frac{dp}{dx}\Big) - kh + 3\alpha\Big[3\Big(\frac{dp}{dx}\Big)^3 h^2 - 6\Big(\frac{dp}{dx}\Big)^2 kh^3 + \frac{9}{2}\Big(\frac{dp}{dx}\Big)k^2h^5\Big]\Bigg]. \end{aligned} \tag{18}$$

The volume flow rate q in the fixed frame is given by

$$q = \int_0^h u\,dy.$$

On evaluating the above integral, the following expression for the volume flux q is obtained.

$$\begin{aligned} q = -h - \frac{dp}{dx}\frac{h^3}{6} + \frac{kh^4}{8} - \frac{3\alpha}{5}\left(\frac{dp}{dx}\right)^3 h^5 - \frac{3\alpha}{12}\left(\frac{dp}{dx}\right)^2 h^6 - \frac{3\alpha}{32}\left(\frac{dp}{dx}\right)k^2h^8 \\ -\beta_1\left[\left(\frac{dp}{dx}\right)h^2 - \frac{k}{2}h^3 + 3\alpha\left(\left(\frac{dp}{dx}\right)^3 h^4 - \frac{9}{2}\left(\frac{dp}{dx}\right)^2 kh^5 + \frac{9}{4}\left(\frac{dp}{dx}\right)k^2h^7\right)\right] \\ -\beta_2\left[\left(\frac{dp}{dx}\right)h - kh^2 + 9\alpha\left(\left(\frac{dp}{dx}\right)^3 h^3 - 2\left(\frac{dp}{dx}\right)^2 kh^4 + \frac{9}{2}\left(\frac{dp}{dx}\right)k^2h^6\right)\right]. \end{aligned} \tag{19}$$

After simplification, we obtain the following relation between the volume flux and the pressure gradient.

$$\begin{aligned} \frac{6(q+h)}{h^3} = -\frac{dp}{dx} + \frac{3kh}{4} - \frac{18\alpha}{5}\left(\frac{dp}{dx}\right)^3 h^2 - \frac{3\alpha}{2}\left(\frac{dp}{dx}\right)^2 kh^3 - \frac{9\alpha}{16}\left(\frac{dp}{dx}\right)k^2h^5 \\ - \frac{6\beta_1}{h^3}\left[\left(\frac{dp}{dx}\right)h^2 - \frac{k}{2}h^3 + 3\alpha\left(\left(\frac{dp}{dx}\right)^3 h^4 - \frac{9}{2}\left(\frac{dp}{dx}\right)^2 kh^5 + \frac{9}{4}\left(\frac{dp}{dx}\right)k^2h^7\right)\right] \\ - \frac{6\beta_2}{h^3}\left[\left(\frac{dp}{dx}\right)h - kh^2 + 9\alpha\left(\left(\frac{dp}{dx}\right)^3 h^3 - 2\left(\frac{dp}{dx}\right)^2 kh^4 + \frac{9}{2}\left(\frac{dp}{dx}\right)k^2h^6\right)\right]. \end{aligned} \tag{20}$$

Eqn (19) yields the pressure gradient equation when Eqn (20) is used.

$$\begin{aligned}\frac{dp}{dx} &= \frac{-6(q+h)}{h^3} + \frac{3kh}{4} - \frac{18\alpha}{5}(\frac{dp}{dx})^3 h^2 - \frac{3\alpha}{2}(\frac{dp}{dx})^2 kh^3 - \frac{9\alpha}{16}(\frac{dp}{dx})k^2h^5 \\ &- \frac{6\beta_1}{h^3}\left[(\frac{dp}{dx})h^3 - \frac{k}{2}h^3 + 3\alpha\Big((\frac{dp}{dx})^3h^4 - \frac{9}{2}(\frac{dp}{dx})^2kh^5 + \frac{9}{4}(\frac{dp}{dx})k^2h^7\Big)\right] \\ &- \frac{6\beta_2}{h^3}\left[(\frac{dp}{dx})h - kh^2 + 9\alpha\Big((\frac{dp}{dx})^3h^3 - 2(\frac{dp}{dx})^2kh^4 + \frac{9}{2}(\frac{dp}{dx})k^2h^6\Big)\right].\end{aligned} \tag{21}$$

Eqn (21) reduces to the Shapiro et al. [26] conclusion in the limiting situation, when $\alpha- > 0$. The nonlinear first-order equation for the pressure gradient is given by

$$\frac{6(q+h)}{h^3} = -\frac{dp}{dx} + \frac{3kh}{4} - \frac{6\beta_1}{h^3}\left[\left(\frac{dp}{dx}\right)h^2 - \frac{k}{2}h^3\right] - \frac{6\beta_2}{h^3}\left[\left(\frac{dp}{dx}\right)h - kh^2\right]. \tag{22}$$

Rearranging terms, we obtain

$$\frac{dp}{dx} = \frac{6(q+h)/h^3 - 3kh/4 + 3\beta_1 k + 6\beta_2 k/h}{-(1+6\beta_1/h + 6\beta_2/h^2)}. \tag{23}$$

It is difficult to obtain an analytic solution for pressure in Eqn (23), as it is a first-order nonlinear equation. However, Eqn (23) may be roughly represented by a perturbation expansion as follows for small values of the pseudoplasticity parameter ($\alpha << 1$).

$$p = p_0 + \alpha p_1. \tag{24}$$

Since the nonlinear terms in the denominator are small, we apply a binomial expansion: i.e., $(1+x)^{-1} \approx 1 - x for |x| << 1$.

$$(1+6\beta_1/h + 6\beta_2/h^2)^{-1} \approx 1 - \frac{6\beta_1}{h} - \frac{6\beta_2}{h^2}. \tag{25}$$

Multiplying the numerator by this series and keeping terms up to first order, we can separate the leading-order and first-order correction:

$$\frac{dp_0}{dx} = -\frac{6(q+h)}{h^3} + \frac{3kh}{4} + 3\beta_1 k + \frac{6\beta_2 k}{h}, \tag{26}$$

$$\frac{dp_1}{dx} = \frac{36\beta_2(q+h)}{h^5} + \frac{36\beta_1(q+h)}{h^4} - \frac{36\beta_2^2 k}{h^3} - \frac{54\beta_1\beta_2 k}{h^2} - \left(18\beta_1^2 + \frac{9}{2}\beta_2\right)\frac{k}{h} - \frac{9}{2}\beta_1 k. \tag{27}$$

Therefore, the approximate pressure gradient is expressed as

$$\frac{dp}{dx} \approx \frac{dp_0}{dx} + \alpha\frac{dp_1}{dx}. \tag{28}$$

where $\alpha \ll 1$ is the pseudoplasticity parameter. This approach clearly separates the Newtonian contribution, wall slip effects, and first-order pseudoplastic corrections, and provides a tractable approximation for the pressure distribution in the channel. Then the overall equation is represented by

$$\frac{dp}{dx} = -\frac{6(q+h)}{h^3} + \frac{3}{4}kh + 3\beta_1 k + 6\beta_2 k\frac{1}{h} + \alpha(\frac{36\beta_2(q+h)}{h^5} + \frac{36\beta_1(q+h)}{h^4} \tag{29}$$

$$- 36\beta_2^2 k\frac{1}{h^3} - 54\beta_1\beta_2 k\frac{1}{h^2} - (18\beta_1^2 + \frac{9}{2}\beta_2)k\frac{1}{h} - \frac{9}{2}\beta_1 k). \tag{30}$$

6 Pumping Characteristics

The following is the equation for the pressure increase per wavelength:

$$\Delta P = \int_0^1 \frac{dp}{dx} dx, \tag{31}$$

$$\Delta P = \int_0^1 (-\frac{6(q+h)}{h^3} + \frac{3}{4}kh + 3\beta_1 k + 6\beta_2 k\frac{1}{h} + \alpha(\frac{36\beta_2(q+h)}{h^5} + \frac{36\beta_1(q+h)}{h^4} - 36\beta_2^2 k\frac{1}{h^3} - 54\beta_1\beta_2 k\frac{1}{h^2} - (18\beta_1^2 + \frac{9}{2}\beta_2)k\frac{1}{h} - \frac{9}{2}\beta_1 k))dx. \tag{32}$$

The following is the expression for the dimensionless frictional force at the wall over a wavelength:

$$F = \int_0^1 h(-\frac{dp}{dx})dx. \tag{33}$$

7 Result and Discussion

The Rabinowitsch fluid's flow properties are determined by the pseudo-plasticity parameter (α). Shear-thickening (dilatant) for $\alpha < 0$, shear-thinning (pseudoplastic) for $\alpha > 0$, and Newtonian fluid for $\alpha = 0$.

The velocity profile for various values of the first-order slip parameter β_1 is shown in Figure 2. The depicted curves show how slip affects the velocity distribution and correspond to ($\beta_1 = 0.1, 0.2, 0.3, 0.4$). The velocity profile changes higher as β_1 rises, suggesting that velocity is increasing throughout the domain. This behavior implies that an overall increase in fluid velocity results from greater slip circumstances. The figure arrow indicates the direction of rising β_1, highlighting the gradual increase in velocity as slip values increase. This pattern suggests that increased slip at the interface facilitates fluid motion by lowering resistance. Sivaranjani & Kavitha [28] reported that increasing slip parameters improves pumping efficiency in pseudoplastic fluids with suction and injection.

Additionally, the velocity profile for various values of the second-order slip parameter β_2 is shown in Figure 3. The shown curves show how the second-order slip condition affects the velocity distribution and correspond to ($\beta_2 = 0.5, 0.6, 0.7, 0.8$). The velocity profile changes higher as β_2 rises, signifying an overall increase in velocity. According to this pattern, fluid motion is improved by lowering boundary resistance when the second-order slip parameter is increased. The figure arrow indicates the direction of rising β_2, demonstrating the gradual increase in velocity. The influence of second-order slip β_2 is depicted. Higher β_2 values correspond to increased velocity, consistent with Aly and Ebaid [5], who demonstrated the significant impact of second-order slip on velocity in nanofluid peristaltic flows. Ramamoorthy and Pallavarapu [22] also found that second-order slip enhances flow characteristics in porous inclined channels.

Reduced wall friction in the Rabinowitsch fluid is shown by an increase in the velocity as both the slip parameters β_1 and β_2 rise. Smoother fluid motion is made possible by increased slip at the borders, which encourages more effective peristaltic transfer.

The velocity profile for various values of the permeability parameter k is shown in Figure 4. Plotting curves for ($k = 0.15, 0.25, 0.35, 0.45$) demonstrate how permeability affects the velocity distribution. Higher wall permeability, which makes it easier for fluid to flow through the porous material, causes the velocity profile to move upward as k rises. Figure 4 shows the effect of wall permeability k on the velocity profile. Higher permeability leads to increased fluid velocities due to easier flow through the wall, which agrees with Ei Shehawey and Husseny [9], Misra and Maiti [18], who reported similar enhancements in velocity and pumping in channels.

The velocity profile for various values of the amplitude ratio ϕ is shown in Figure 5. The curves corresponding to ($\phi = 0.40, 0.50, 0.60$, and 0.70) illustrate how changes in ϕ affect the velocity distribution. The upward trend of the curves indicates that increasing ϕ leads to higher velocity. This implies that a larger amplitude ratio enhances the wave-induced pumping efficiency, thereby increasing the fluid velocity. Increasing ϕ results in higher velocities, consistent with the classic work of Shaprio et al [26], where higher occulsion ratios enhance velocity and pressure in Newtonian peristaltic flows. More recent studies, reported that higher occlusion ratios enhance pumping efficiency in peristalsis, and with Misra and Maiti [18], who showed that suction and injection significantly modify velocity fields in porous channels, improving fluid transport.

For various values of the slip parameter ($\beta_1 = 0.1, 0.2, 0.3, 0.4$), Figure 6 shows this pattern, emphasised by the arrow in the picture, which indicates that the pressure difference rises as β_1 does. According to this behavior, a more effective peristaltic transport mechanism under regulated circumstances is made possible by raising the slip parameter, which also raises the flow resistance. As β_1 increases, both the velocity and pressure difference exhibit a noticeable rise. This trend aligns with findings by Goud and Reddy [11], who reported similar enhancements in pressure difference within increasing slip parameters in Rabinowitsch fluid models.

The pressure flow connection for different values of the slip parameter β_2 is shown in Figure 7 ($\beta_2 = 0.6, 0.7, 0.8, 0.9$), which illustrates how variations in β_2 impact the pressure-flow properties in peristaltic transport. Physically, this behavior suggests that a rise in β_2 increases viscous dissipation because of improved slip conditions and permits the fluid to flow more freely over the channel walls.

Greater resistance to flow is shown by an increase in the pressure difference as the slip parameters β_1 and β_2 rise. This illustrates how boundary slip affects flow control and how crucial slip conditions are to the design of effective peristaltic pumping systems. This observation is consistent with the results presented by Aly and Ebaid [5], nothing that higher values of β_2 correspond to increased flow rates and pressure differences in peristaltic transport of non-Newtonian fluids. Figure 8 shows how the pressure difference changes when the amplitude ratio (ϕ) varies. According to the presented graphs, which correspond to ($\phi = 0.55, 0.56, 0.57, 0.58$), the pressure difference at a fixed flow rate rises as ϕ increases. This suggests that in peristaltic transport, a greater wave amplitude needs greater pressure to maintain the same volumetric flow rate. This behavior is in agreement with the study by Maiti and Misra [18], who observed that a higher amplitude ratio results in a greater pressure difference in peristaltic transport of non-Newtonian fluids.

The pressure difference for various suction and injection parameter values (k) is shown in Figure 9. The graphs show that at a fixed flow rate, the pressure differential grows as k increases. They correspond to ($k = 0.10, 0.15, 0.20, 0.25$). This behavior implies that additional resistance is introduced by increasing wall permeability, necessitating higher pressure to sustain fluid movement. This trend is supported by the findings of Abd-Alla et al. [2], who reported that higher values of k leads to increased pressure differences in peristaltic transport of non-Newtonian fluids.

In Rabinowitsch fluid transport in a peristaltic channel, increased slip, wall porosity, and wave amplitude all work together to raise the pressure needed to keep the volumetric flow rate constant. Figures 10 to 13 show that when the pressure rate changes, the frictional force is just opposite behavior to the pressure rate.

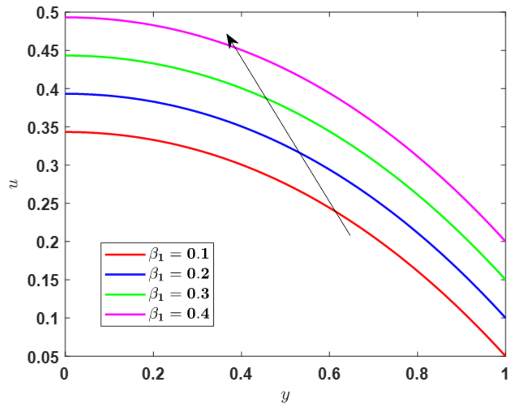

Figure 2: Velocity profile for different β_1 with $\alpha = 0.01$, $k = 0.25$, $\phi = 0.56.\beta_2 = 0.9$

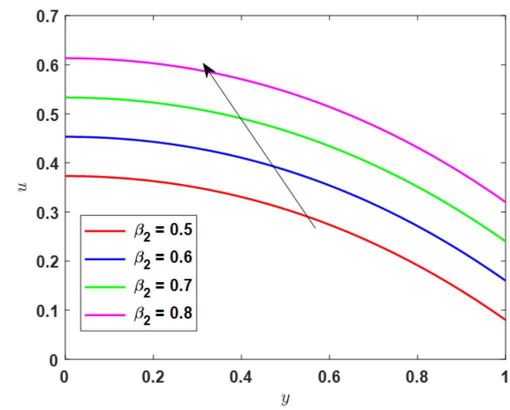

Figure 3: Velocity profile for different β_2 with $\alpha = 0.01$, $k = 0.25$, $\phi = 0.56.\beta_1 = 0.2$.

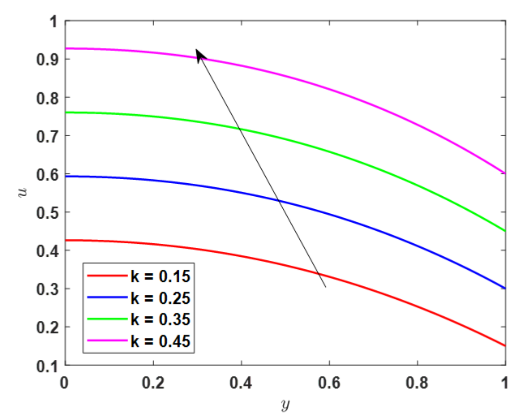

Figure 4: Velocity profile for different k with $\alpha = 0.01$, $\phi = 0.56$,$\beta_1 = 0.2$,$\beta_2 = 0.9$.

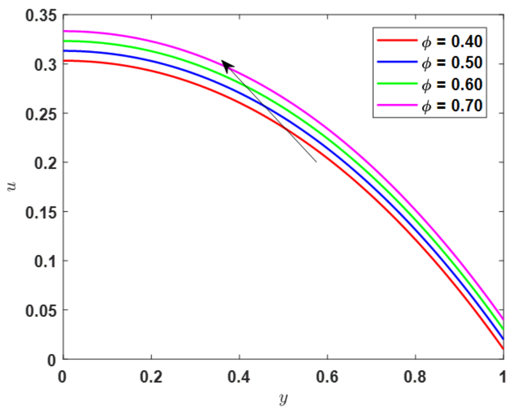

Figure 5: Velocity profile for different ϕ with $\alpha = 0.01$, k=0.25,$\beta_1 = 0.2$,$\beta_2 = 0.9$.

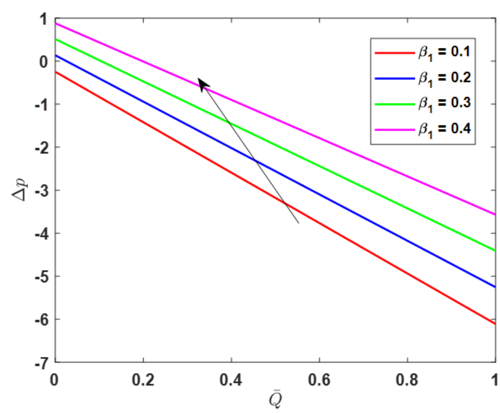

Figure 6: The distinction between Δp and $\bar{Q}$ for β_1 with $\beta_2 = 0.4$ $k = 0.3$, $\alpha = 0.07$, and $\phi = 0.35$.

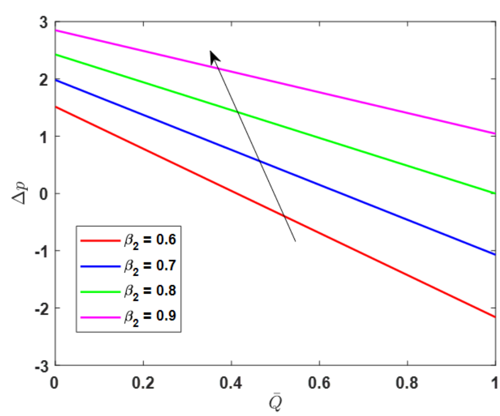

Figure 7: The distinction between Δp with $\bar{Q}$ for β_2 with $\beta_1 = 0.3$, $\alpha = 0.07$, $\phi = 0.35$, k=0.3.

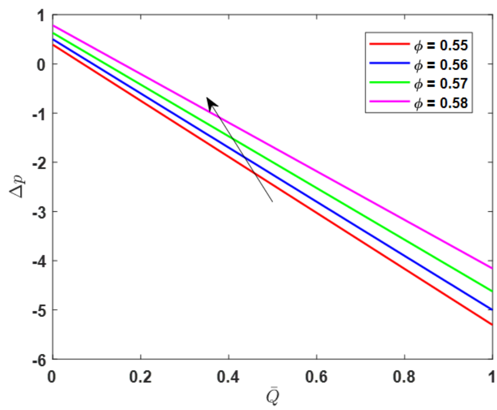

Figure 8: The distinction between Δp with $\bar{Q}$ for ϕ with $\beta_1 = 0.4$, $\beta_2 = 0.3$, $\alpha = 0.07$, k=0.5.

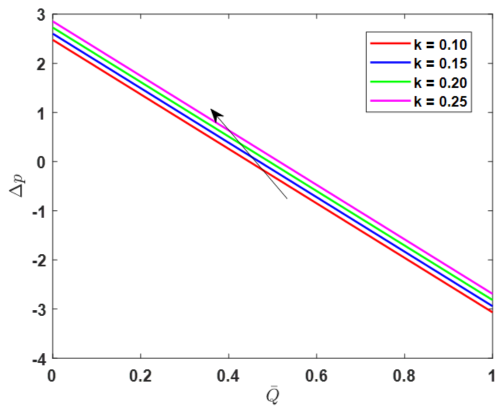

Figure 9: The distinction between Δp with $\bar{Q}$ for k with $\beta_1 = 0.3$, $\alpha = 0.07$, $\phi = 0.35$, $\beta_2 = 0.3$

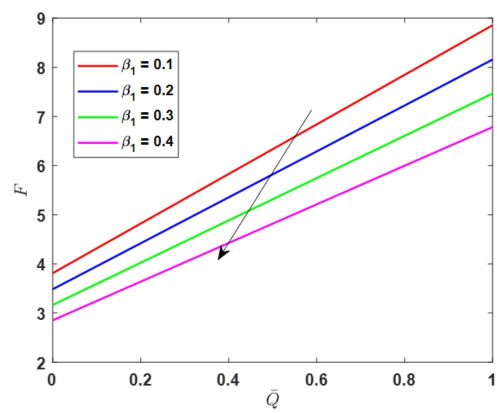

Figure 10: The distinction between F with $\bar{Q}$ for β_1 with $\beta_2 = 0.4$ $k = 0.3$, $\alpha = 0.07$, $\phi = 0.35$.

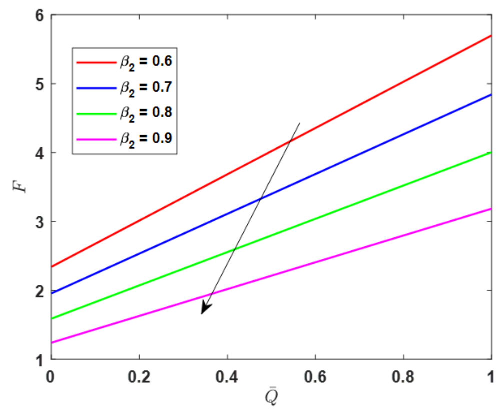

Figure 11: The distinction between F with $\bar{Q}$ for β_2 with $\beta_1 = 0.3$, $\alpha = 0.07$, $\phi = 0.35$, k=0.3.

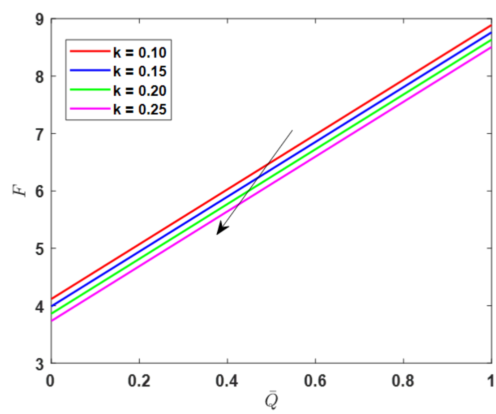

Figure 12: The distinction between F with $\bar{Q}$ for k with $\beta_1 = 0.3$, $\alpha = 0.07$, $\phi = 0.35$, $\beta_2 = 0.3$

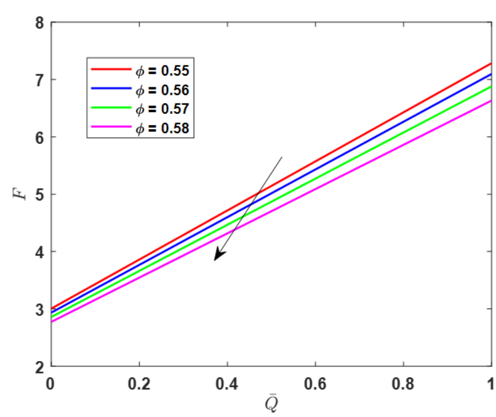

Figure 13: The distinction between F with $\bar{Q}$ for ϕ with $\beta_1 = 0.4$, $\beta_2 = 0.3$, $\alpha = 0.07$, k=0.3.

8 Conclusion

In this work, the peristaltic transport of a Rabinowitsch fluid with slip effects was analyzed, and analytical formulations for pressure, velocity, and frictional force were obtained using lubrication theory principles valid for slow, wave-driven flows. The impact of important parameters on the flow characteristics was examined through MATLAB simulations. The results can be summarized as follows:

1. Reduced wall friction in the Rabinowitsch fluid is demonstrated by an increase in the velocity profile as both slip parameters β_1 and β_2 rise. Enhanced slip at the boundaries facilitates smoother fluid motion, resulting in more effective peristaltic transfer.
2. The velocity profile increases with the suction/injection parameter and the amplitude ratio ϕ, indicating improved fluid transport. Stronger wall contact and higher wave amplitude promote enhanced propulsion of the Rabinowitsch fluid under peristaltic motion.
3. The pressure differential rises with increasing slip parameters β_1, β_2, amplitude ratio ϕ, and permeability k, signifying greater flow resistance. In Rabinowitsch fluid transport, enhanced slip, wall porosity, and wave amplitude necessitate higher pressure to maintain a steady volumetric flow rate.
4. The frictional force exhibits an opposite behavior to the pressure rate.

Overall, this study provides theoretical insights into the role of slip, suction/injection, and permeability in controlling peristaltic transport of Rabinowitsch fluid. The findings hold significant relevance in biomedical applications such as blood circulation, chyme propulsion, and urine transport, as well as in industrial processes involving polymer solutions, drug delivery systems, and energy-efficient fluid handling.

9 APPLICATION

There are several useful applications in the biological and industrial domains for the investigation of peristaltic transport of Rabinowitsch fluid with suction and injection under slip circumstances. It aids in the design of artificial organs, the optimisation of drug delivery systems, and the comprehension of blood flow dynamics in small arteries in biomedical engineering. Similar to this, these flow models are helpful for physiological processes including the flow of synovial fluid in joints, urine transport via the ureters, and blood movement in capillaries with porous walls. The effects of suction/injection mechanisms and slip conditions are important in drug delivery systems because focused therapy requires precise fluid management. The study is especially pertinent to the movement of fluids throughout the gastrointestinal tract, where peristaltic action is essential. These findings are valuable for applications such as enhanced oil extraction, microscale fluid manipulation, and polymer-based process optimization. The study is also helpful for developing lubrication and cooling systems, where efficient fluid transport management is required under a variety of circumstances. Its significance in engineering applications can be further increased by using the effects of suction and injection on fluid velocity in filtering systems and membrane-based separation procedures. This research is crucial for the design of filtration systems, polymer processing, and microfluidic devices where non-Newtonian fluids behave as dilatants or pseudoplastics. Comprehending how slip effects interact with suction and injection can improve the effectiveness of lubricating systems, membrane-based fluid separation procedures, and chemical and bioreactors.

Acknowledgments The authors declare that there are no acknowledgments for this work.

Conflicts of interest Conflicts of interest are not disclosed.

Data availability No Data availabality statement is occured.

References

[1] Z. Abbas, M. Y. Rafiq, J. Hasnain & H. Umer (2021). Impacts of lorentz force and chemical reaction on peristaltic transport of jeffrey fluid in a penetrable channel with injection/suction at walls. *Alexandria Engineering Journal*, *60*(1), 1113–1122. https://doi.org/10.1016/j.aej.2020.10.035.

[2] A. M. Abd-Alla, S. M. Abo-Dahab, D. M. Salah, F. S. Bayones & M. A. Abdelhafez (2023). Magneto-hydrodynamic peristaltic flow of a jeffery fluid in the presence of heat transfer through a porous medium in an asymmetric channel. *Scientific Reports*, *13*(1), 21088. https://doi.org/10.1038/s41598–023–48137–x.

[3] N. S. Akbar & A. W. Butt (2015). Heat transfer analysis of rabinowitsch fluid flow due to metachronal wave of cilia. *Results in Physics*, *5*, 92–98. https://doi.org/10.1016/j.rinp.2015.03.005.

[4] S. Akram, M. Hanif & S. Nadeem (2014). Peristaltic transport of a maxwell fluid in a porous asymmetric channel through a porous medium. *Cogent Engineering*, *1*(1), 980770. https://doi.org/10.1080/23311916.2014.980770.

[5] E. H. Aly & A. Ebaid (2014). Effect of the velocity second slip boundary condition on the peristaltic flow of nanofluids in an asymmetric channel: exact solution. *Abstract and Applied Analysis*, *2014*, 191876. https://doi.org/10.1155/2014/191876.

[6] K. Chakradhar, K. Nandagopal, V. Prashanthi, A. Parandhama, T. Somaiah, B. V. S. Thrinath, N. Tarakaramu, G. Rasool & D. Abduvalieva (2025). Mhd effect on peristaltic motion of williamson fluid via porous channel with suction and injection. *Partial Differential Equations in Applied Mathematics*, *13*, 101103. https://doi.org/10.1016/j.padiff.2025.101103.

[7] A. J. Chamkha, A. M. Aly & M. A. Mansour (2010). Similarity solution for unsteady heat and mass transfer from a stretching surface embedded in a porous medium with suction/injection and chemical reaction effects. *Chemical Engineering Communications*, *197*(6), 846–858. https://doi.org/10.1080/00986440903359087.

[8] M. M. Channakote & D. V. Kalse (2021). Heat transfer in peristaltic motion of rabinowitsch fluid in a channel with permeable wall. *Applications & Applied Mathematics*, *16*(2).

[9] E. F. El Shehawey & S. Z. A. Husseny (2000). Effects of porous boundaries on peristaltic transport through a porous medium. *Acta Mechanica*, *143*(3), 165–177. https://doi.org/10.1007/BF01170946.

[10] Y. Elmhedy, A. M. Abd-Alla, S. M. Abo-Dahab, F. M. Alharbi & M. A. Abdelhafez (2024). Influence of inclined magnetic field and heat transfer on the peristaltic flow of rabinowitsch fluid model in an inclined channel. *Scientific Reports*, *14*(1), 4735. https://doi.org/10.1038/s41598–024–54396–z.

[11] J. S. Goud & R. H. Reddy (2017). Peristaltic transport of a pseudoplastic fluid bounded by permeable walls with suction and injection. *International Journal of Pure and Applied Mathematics*, *113*(6), 289–297.

[12] T. Hayat, S. Hina & N. Ali (2010). Simultaneous effects of slip and heat transfer on the peristaltic flow. *Communications in Nonlinear Science and Numerical Simulation*, *15*(6), 1526–1537. https://doi.org/10.1016/j.cnsns.2009.06.032.

[13] N. Ismail, N. Ariffin, R. Nazar & N. Bachok (2019). Stability analysis of stagnation-point flow and heat transfer over an exponentially shrinking sheet with heat generation. *Malaysian Journal of Mathematical Sciences*, *13*(2), 107–122.

[14] F. Kamışlı (2006). Laminar flow of a non-newtonian fluid in channels with wall suction or injection. *International Journal of Engineering Science*, *44*(10), 650–661. https://doi.org/10.1016/j.ijengsci.2006.04.003.

[15] K. T. Kumar & A. Kavitha (2017). The influence of slip effects on peristaltic transport of a rabinowitsch fluid model in a non uniform tube. In *IOP Conference Series: Materials Science and Engineering*, volume 263 pp. 062004. https://doi.org/10.1088/1757–899X/263/6/062004.

[16] J.-R. Lin, L.-M. Chu, T.-C. Hung & P.-Y. Wang (2016). Derivation of two-dimensional non-newtonian reynolds equation and application to power-law film slider bearings: Rabinowitsch fluid model. *Applied Mathematical Modelling*, *40*(19-20), 8832–8841. https://doi.org/10.1016/j.apm.2016.04.030.

[17] S. Maiti & J. C. Misra (2013). Non-newtonian characteristics of peristaltic flow of blood in micro-vessels. *Communications in Nonlinear Science and Numerical Simulation*, *18*(8), 1970–1988. https://doi.org/10.1016/j.cnsns.2012.12.015.

[18] J. C. Misra, S. Maiti & G. C. Shit. Peristaltic transport of a physiological fluid in an asymmetric porous channel in the presence of an external magnetic field. *Journal of Mechanics in Medicine and Biology*, *8*(4), 507–525. https://doi.org/10.1142/S0219519408002784.

[19] J. C. Misra & S. K. Pandey. Peristaltic transport of a non-newtonian fluid with a peripheral layer. *International Journal of Engineering Science*, *37*(14), 1841–1858. https://doi.org/10.1016/S0020–7225(99)00005–1.

[20] M. Y. Rafiq & Z. Abbas. Impacts of viscous dissipation and thermal radiation on rabinowitsch fluid model obeying peristaltic mechanism with wall properties. *Arabian Journal for Science and Engineering*, *46*(12), 12155–12163. https://doi.org/10.1007/s13369–021–05870–7.

[21] C. Rajashekhar, H. Vaidya, K. V. Prasad, I. Tlili, A. Patil & P. Nagathan (2020). Unsteady flow of rabinowitsch fluid peristaltic transport in a non-uniform channel with temperature-dependent properties. *Alexandria Engineering Journal*, *59*(6), 4745–4758. https://doi.org/10.1016/j.aej.2020.08.036.

[22] M. Ramamoorthy & L. Pallavarapu (2022). Second order slip flow of a conducting jeffrey nanofluid in an inclined asymmetric porous conduit with heat and mass transfer. *Multidiscipline Modeling in Materials and Structures*, *18*(6), 1016–1038. https://doi.org/10.1108/MMMS–08–2022–0149.

[23] H. Sadaf & S. Nadeem (2017). Analysis of combined convective and viscous dissipation effects for peristaltic flow of rabinowitsch fluid model. *Journal of Bionic Engineering*, *14*(1), 182–190. https://doi.org/10.1016/S1672–6529(16)60389–X.

[24] R. Saravana, K. Vajravelu & S. Sreenadh (2018). Influence of compliant walls and heat transfer on the peristaltic transport of a rabinowitsch fluid in an inclined channel. *Zeitschrift für Naturforschung A*, *73*(9), 833–843. https://doi.org/10.1515/zna–2018–0181.

[25] N. Satwai, K. M. Prasad & M. V. Phani Kumari (2025). Analysis of blood flow with nanoparticles through a porous inclined overlapping stenosed artery under the influence of external magnetic field. *Malaysian Journal of Mathematical Sciences*, *19*(3), 1–??. https://doi.org/10.47836/mjms.19.3.01.

[26] A. H. Shapiro, M. Y. Jaffrin & S. L. Weinberg (1969). Peristaltic pumping with long wavelengths at low reynolds number. *Journal of Fluid Mechanics*, *37*(4), 799–825. https://doi.org/10.1017/S0022112069000899.

[27] U. P. Singh, A. Medhavi, R. S. Gupta & S. S. Bhatt (2018). Theoretical study of heat transfer on peristaltic transport of non-newtonian fluid flowing in a channel: Rabinowitsch fluid model. *International Journal of Mathematical, Engineering and Management Sciences*, *3*(4), 450–471.

[28] S. Sivaranjani & A. Kavitha (2025). Impact of first order slip condition on peristaltic transport of a pseudoplastic fluid under mhd effect bounded by permeable walls with suction and injection. *Contemporary Mathematics*, pp. 1091–1109. https://doi.org/10.37256/cm.6120255786.

[29] S. Srinivas, R. Gayathri & M. Kothandapani (2009). The influence of slip conditions, wall properties and heat transfer on mhd peristaltic transport. *Computer Physics Communications*, *180*(11), 2115–2122. https://doi.org/10.1016/j.cpc.2009.06.015.

[30] D. Tripathi (2011). Peristaltic transport of a viscoelastic fluid in a channel. *Acta Astronautica*, *68*(7-8), 1379–1385. https://doi.org/10.1016/j.actaastro.2010.09.012.

[31] H. Vaidya, C. Rajashekhar, G. Manjunatha & K. V. Prasad (2019). Effect of variable liquid properties on peristaltic flow of a rabinowitsch fluid in an inclined convective porous channel. *The European Physical Journal Plus*, *134*(5), 231. https://doi.org/10.1140/epjp/i2019–12536–y.

[32] C. Yu-Ming, N. Mubbashar, K. M. Ijaz, A. Waqas, Z. Zareen, K. Seifedine & A. Zahra (2020). Entropy analysis in the rabinowitsch fluid model through inclined wavy channel: Constant and variable properties. *International Communications in Heat and Mass Transfer*, pp. 104980. https://doi.org/10.1016/j.icheatmasstransfer.2020.104980.